International Journal of Engineering

Journal Homepage: www.ije.ir

Structural, Optical and Defect State Analyses of ZnO Nanoparticle Films

S. Y. Purwaningsih, M. Zainuri, T. Triwikantoro, S. Pratapa, D. Darminto*

Department of Physics, Faculty of Science, Institute Teknologi Sepuluh Nopember (ITS), Surabaya, Indonesia

PAPER INFO

Paper history:
Received 03 November 2019
Received in revised form 24 January 2020
Accepted 07 March 2020

Keywords:
ZnO Nanoparticle
Co-precipitation
Thick Film
Optical Property
Defect State

ABSTRACT

Synthesis of ZnO nanostructures films by a co-precipitation followed by the deposition processed onto a glass substrate by spin-coating technique was carried out. The effect of annealing temperatures (from 250 to 325 °C for 30 min) on the structural and optical properties of the ZnO films have been investigated. The structural studies reveal that ZnO films are polycrystalline with hexagonal wurtzite structure. The X-ray diffraction (XRD) data show a better crystallinity at (101) crystal plane for the annealed films at 300 °C than the other ZnO films. The average grain size increases (from 31 to 36 nm) with an increase in annealing temperatures. The band gap energy is approximately 3.40 eV for the as-prepared films and varies from 3.25 to 3.18 eV with an increase in annealing temperatures. The photoluminescence (PL) results show a weak ultraviolet and relatively broad visible emissions respect to various defect structures in the ZnO films, in which the interstitial and vacancy oxygen are the main factors influencing the electronic properties in the whole ZnO films.

***doi**: 10.5829/ije.2020.33.05b.17*

NOMENCLATURE

β_{hkl}	The full width at half maximum (FWHM-in radian) intensity	V_o^{++}	The doubly ionized oxygen vacancy
$(\beta_{hkl})_{measured}$	The width of the half-maximum intensity	O_{Zn}	Oxygen antisite
$(\beta_{hkl})_{instrumental}$	The instrumental corrected broadening	O_i	Interstitial oxygen
D	The crystallite size or grain size (nm)	V_{Zn}	Zinc vacancies
V	Unit cell volume (nm^3)	Zn_i	Zinc interstitial
a	Lattice parameter (Å)	**Greek Symbols**	
c	Lattice parameter (Å)	λ	The incident wavelength (nm)
B	A constant which has different values for different transitions	h	Planck constant (J.s)
E_g	Band gap energy (eV)	ν	Velocity of light (m/s)
E_i	A constant	θ	The Bragg diffraction angle (degree)
E_{tail}	Urbach energy (eV)	α	The absorption coefficient
V_o	Oxygen vacancy	α_o	A constant that characterize the materials
V_o^0	The neutral oxygen vacancy	**Subscripts**	
V_o^+	The singly ionized oxygen vacancy	hkl	Miller indices

1. INTRODUCTION

Nanoscale materials are considerably attractive compared with their bulk forms because of their unique properties as a result of the large specific surface area and quantum effects. Many researches have indicated that the physical and chemical responses can easily be controlled by their shape and/or size of the materials within the range of 1–100 nm [1]. Among the various nanostructured materials, ZnO nanoparticles have

*Corresponding Author Email: *darminto@physics.its.ac.id* (D. Darminto)

Please cite this article as: S. Y. Purwaningsih, M. Zainuri, Triwikantoro, S. Pratapa, Darminto, Structural, Optical and Defect State Analyses of ZnO Nanoparticle Films, International Journal of Engineering (IJE), IJE TRANSACTIONS B: Applications Vol. 33, No. 5, (May 2020) 852-860

become the most promising materials due to their various applications. ZnO crystallizes with hexagonal wurtzite-type structure at room temperature. It has a wide band gap (E_g) of 3.37 eV, large exciton binding energy of about 60 meV, and high optical transparency [2]. It has also been used in various fields of applications, for example, light emitting diodes (LED), field emission transistors, photovoltaic devices, room-temperature UV lasers, piezoelectric nanogenerators, and gas sensors [3-7]. The ZnO nanoparticles with a high specific surface area may consist of defect states playing an essential role on their optical and electrical properties [8]. The quantum confinement effect of charge carriers in ZnO nanoparticles can cause widening of the energy band gap, which in turn, affects the ultraviolet (UV) and visible light absorption. The photoluminescence (PL) spectra in the visible light range is mainly due to the surface defects of the crystal, resulting in various of emission peaks depending on the crystal structure [9].

The thin and/or thick films of ZnO nanoparticles have been successfully grown using a number of advanced techniques through vapour deposition techniques such as molecular beam epitaxy (MBE) [10], chemical vapor deposition (CVD) [11], metal-organic chemical vapor deposition (MOCVD) [12], and RF-sputtering [13]. However, these deposition techniques faced drawbacks such as poor flexibility, being expensive, and having complicated growth conditions. Meanwhile, solution deposition techniques such as hydrothermal [14], dip-coating and spin-coating [15−16] have been considered as some alternatives. The spin-coating method is relatively easy, low-cost, and utilizing simpler equipments. Many researchers have also reported the annealing effects on the structure and luminescence properties of the ZnO thin films with enhanced properties [17−18].

In the present work, ZnO nanoparticles were prepared through a simple co-precipitation route using certain acid and base pairs without calcination process. These nanoparticles were then deposited on a glass substrate using spin-coating technique. The films were continued by annealing process. The formation of defects in the films can be controlled with different annealing temperatures. The structural and optical characterizations of these as-prepared and annealed films are analyzed by X-ray diffraction (XRD), scanning electron microscopy (SEM), UV-Vis spectrophotometer, and photoluminescence (PL). These analyzed data were used to investigate the effect of low-annealing temperature on the structural and optical properties as well as the defect states of the ZnO films.

2. MATERIALS AND METHODS

2. 1. Preparation of ZnO Nanoparticles All chemical reagents with analytical grade were used directly without further purification. Zinc diacetate dihydrate ($Zn(CH_3COO)_2{\cdot}2H_2O$) and hydrochloric acid (HCl) were purchased from Merck. The ZnO nanoparticles were prepared by co-precipitation technique. Firstly, 2.219 g of $Zn(CH_3COO)_2{\cdot}2H_2O$ was dissolved in 40 ml of diluted HCl (0.5 M) followed by stirring the solution for 1 h to accommodate homogeneous reaction. The reaction product was then slowly titrated with 40 ml of 0.5 M ammonium hydroxide (NH_4OH) until the solution changed into an emulsion. The ammonia solution was continuously added into the emulsion up to pH value of about 9.5 to obtain a transparent colloidal substance. Next, the mixed solution was heated at 85 °C and stirred for 6 h. After cooling down to room temperature, it was filtered and washed by distilled water for several times. Then, white precipitates were obtained. Finally, the precipitate was dried in an oven at 100 °C for 3 h, then it was collected and ground on the agate mortar.

2. 2. Fabrication of ZnO Nanoparticles Films Ultrasonically cleaned glass slides were used as the substrate. First, the prepared ZnO powders were dissolved in alpha terpineol ($C_{10}H_{18}O$) and then stirred for 1 h to obtain a paste. To enhance the mechanical adhesion of the paste on the glass substrate, a small amount of ethyl cellulose ($C_{20}H_{38}O_{11}$) as an organic binder was added to the mixed powder. Spin coating technique was used to coat the glass substrate with the paste using a rotating speed of 2000 rpm for 30 s. After coating, the film was dried on the hot plate at 225 °C for 15 min to remove the organic binder and to keep strong adhesion between the coated paste and the glass substrate. Finally, as-prepared films were annealed at different temperatures of 250, 275, 300, and 325 °C for 30 min in a furnace.

2. 3. Characterization of ZnO Films The crystal structure of the prepared ZnO films was characterized by X-ray diffractometer (XRD, Rigaku Rint 2000 HV series X-ray automatic diffractometer). The XRD patterns were collected using Cu K_α radiation (λ = 0.154056 nm) operated at 40 kV and 200 mA with diffraction angle (2θ) from 10° to 80° and the scan step of 0.01°. The XRD measurements were performed at room temperature and recorded using the grazing incidence. The surface morphology of the annealed films was analyzed using scanning electron microscope (SEM, JSM-7600F, JEOL). The absorbance spectra were obtained using a ultraviolet-visible spectrophotometer (UV-Vis, Genesys 10S) measured at room temperature in the wavelength range of 200-800 nm with a scan step of 600 nm/min. Photoluminescence spectra (USB-2000, Ocean Optics) were recorded using a He-Cd laser with an excitation wavelength of 325 nm (3.82 eV) at room temperature.

3. RESULTS AND DISCUSSION

3. 1. Structural Analysis of ZnO Films Figure 1 shows the XRD patterns of the ZnO films at various annealing temperatures of 250, 275, 300 and 325 °C in air for 30 min. The sharp diffraction peaks demonstrate that the ZnO films are well crystalline. The positions of diffraction peaks are shown at crystal planes of (100), (002), (101), (102), (110), (103), (200), (112), and (201). All diffraction peaks of the ZnO films are well indexed to be the hexagonal wurtzite structure with space group of P63mc (JCPDS#36-1451) [19−20]. Based on XRD data, there are no other peaks coming from impurity phases of other organics and oxides. This shows that all the films have been grown as ZnO crystals. The presence of several peaks in all samples reflects the random orientation of the crystallites. The XRD data show a well-defined diffraction peaks, which represent that thermally annealed films have good crystallization. It is clear from Figure 1 that the peak intensity of (101) plane increases with an increase in annealing temperatures. The enhancement of peak intensity for the (101) plane from the as-prepared sample and the one annealed at 300 °C indicates that there is a preferred orientation effect during annealing process. The existence of this prominent peak is expected to be related to oxygen vacancies in ZnO crystals [21].

The crystal size of the ZnO film was calculated using the highest peak in the XRD results. The broadening of the diffraction peaks depends on both sample and instruments effects. The instrument correction was estimated using a standard material, namely standard silicon. The corrected instrumental broadening (β_{hkl}) corresponding to the diffraction peak of ZnO films was calculated using the relation in Equation (1) [22].

$$\beta_{hkl} = \left[(\beta_{hkl})^2_{measured} - \left(\beta^2_{instrumental} \right) \right]^{1/2} \quad (1)$$

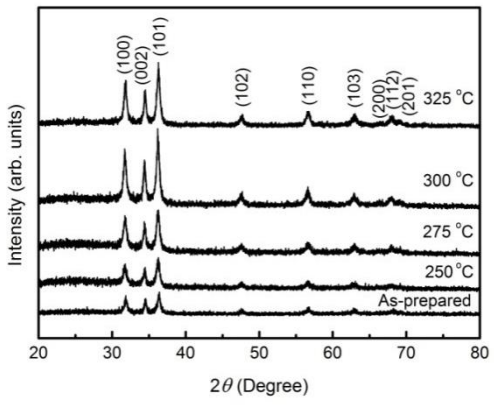

Figure 1. XRD patterns of ZnO films annealed at different temperatures as specified

The average crystallite size of ZnO films can be estimated by Debye-Scherrer formula in Equation (2) [21].

$$D = \frac{0.9\lambda}{\beta_{hkl} \cos\theta} \quad (2)$$

where D is the crystallite size of the nanoparticles, λ is the wavelength (λ = 0.154056 nm), θ is diffraction angle, and β_{hkl} is the full-width at half-maximum (FWHM) of the diffraction peak. The estimated 2θ values, calculated FWHM, and average crystallite size (D) of the samples annealed at different temperatures are listed in Table 1. The numbers in parentheses in Table 1 indicate the calculation error. These results show that the crystallite size increases from 31 nm to 36 nm with increasing the annealing temperatures. This clearly indicates the presence of nano-sized particles in the samples.

The values of lattice parameters (a and c) were obtained from the plane spacing equations for a hexagonal crystal structure [23].

$$\frac{1}{d^2} = \frac{4}{3}\left\{ \frac{h^2 + hk + k^2}{a^2} \right\} + \frac{l^2}{c^2} \quad (3)$$

For the first order approximation n = 1, Bragg's Law: $n\lambda = 2d\sin\theta$ can be rearranged as follows:

$$\sin^2\theta = \frac{\lambda^2}{4d^2} \quad (4)$$

Combining Equations (3) and (4):

$$\frac{1}{d^2} = \frac{4}{3}\left\{ \frac{h^2 + hk + k^2}{a^2} \right\} + \frac{l^2}{c^2} = \frac{4\sin^2\theta}{\lambda^2} \quad (5)$$

$$\sin^2\theta = \left(\frac{\lambda^2}{4a^2} \right) \left[\frac{4}{3}\left\{ h^2 + hk + k^2 \right\} + \frac{l^2}{(c/a)^2} \right] \quad (6)$$

Since lattice parameters and the ratio of the lattice parameters are constant for a given diffraction pattern, is constant for a hexagonal crystal structure. The relationship between the wavelength of X-ray diffraction, the Bragg's angle, the Miller indices (hkl), and the lattice

TABLE 1. Estimated 2θ values, calculated FWHM, and average crystallite size of the ZnO films annealed at different temperatures

Samples	2θ (°)	β_{hkl} (°)	D (nm)
As-prepared	36.358(4)	0.550(17)	31
250 °C	36.237(5)	0.537(24)	32
275 °C	36.237(4)	0.530(14)	33
300 °C	36.228(3)	0.496(10)	35
325 °C	36.289(3)	0.487(11)	36

parameters in hexagonal structures is given in Equation (6). Using Equation (6), we obtain the following equation for the calculation of the values of *a* and *c* for those *hkl* indices.

$$a = \frac{\lambda}{\sqrt{3}\sin\theta}\sqrt{h^2 + hk + k^2} \quad (7)$$

$$c = \frac{\lambda}{2\sin\theta}l \quad (8)$$

The volume of unit cell for the hexagonal structure has been calculated by using Equation (9) [23].

$$V = \frac{\sqrt{3}a^2c}{2} = 0.866a^2c \quad (9)$$

The calculated lattice parameters and unit cell volume are given in Table 2. The lattice parameters for ZnO films prepared and annealed at different temperatures indicate hexagonal unit cells that are very close to the standard lattice parameter values for ZnO with a = 0.3249 nm and c = 0.5206 nm [20]. From Table 2, it is seen that the heat-treated ZnO films have higher a and c values than those of the as-prepared one. The changes in the lattice parameters with increasing annealing temperatures indicate the presence of strain in the lattice of ZnO films. Consequently, it may produce defects related to the optical properties. This will later be discussed further.

Based on Table 1, it can be observed that the Bragg angle of the (101) crystal plane of the annealed ZnO films is slightly shifted towards the lower values compared with that of as-prepared one. This is due to the formation of internal micro-stress. In addition, peak broadening is also observed in the XRD data. It is commonly recognized that the XRD line broadening may be the result of crystallite size, micro-strain, or both of them. Micro strains decrease with increasing annealing temperature because the atoms trapped in the non-equilibrium position tend to shift to more equilibrium position after the annealing process. Therefore, the decrease of micro-strain causes an increase in lattice parameter and crystallite size [22].

3. 2. Surface Morfologi Figures 2(a)-2(e) show the surface morphology of the as-prepared and annealed ZnO films. The SEM images clearly observe that the average particle size is in the order of nanometer. Some agglomerations along with individual particles are also seen in Figure 2.

TABLE 2. Lattice parameters and unit cell volume of the ZnO films at various annealing temperatures

Samples	*a* (nm)	*c* (nm)	*D* (nm)
As-prepared	0.3243(6)	0.5193(13)	31
250 °C	0.3253(4)	0.5212(6)	32
275 °C	0.3253(4)	0.5210(4)	33
300 °C	0.3254(5)	0.5212(6)	35
325 °C	0.3249(1)	0.5202(4)	36

Figure 2(a) shows that the as-prepared ZnO particles are relatively homogeneous and distributed almost uniform on the substrate surface. The particles contain irregular and spherical-like shape with grain size of around 20-32 nm, which is in agreement with the XRD data. The grain size increases with an increase in annealing temperatures.

Figure 2(b) shows that the surface morphology of the sample after annealing at 250 °C has slightly larger grain size than that of the as-prepared ZnO films. The shape of the particles is formed as an irregular spherical-like structure with grain size of around 30-40 nm. The surface morphology with a larger grain size of around 35-45 nm occurs by increasing the annealing temperature as shown in Figure 2(d). In addition, the annealing temperature provides a reduction of grain boundaries and consequently particles size increases. The annealing process induces a dominant effect on the morphology and the microstructure of the films. As the temperature rises, the ZnO films show similar morphologies.

In general, the high annealing temperature will induce low degree of crystallinity due to the existence of possible disorder/defects in the films. The high temperature may provide the crystal growth of ZnO with a high driving force to overcome the anisotropic crystal growth. This driving force affects the surface energy controlling the size and morphology of the grains. During the annealing process, the nucleation phase will influence the obtained morphologies of both shape and size of the grains.

3. 3. Optical Properties Figure 3 displays the absorption spectra of the films as a function of wavelength. For the as-prepared film and the films annealed at 250-275 °C show absorption peaks located at 370 nm. Meanwhile, the absorption peak of the films annealed at 300-325 °C shifts slightly to a longer wavelength at 375 nm (red-shift). These shifts correspond to the change in the optical band gap of the annealed films. All films show relatively strong absorption peaks. The intensity of the absorption peak in the absorbance spectra is associated with the crystalline quality of the ZnO films. The crystallinity of the films, the type, and the density of defects will affect the crystalline quality. Therefore, the appropriate absorption peak intensity is different.

The band gap energy with direct allowed transition can be determined using the Tauc relationship. It is given by the following expression in Equation (10) [24].

$$(\alpha h\nu)^2 = B(h\nu - E_g) \quad (10)$$

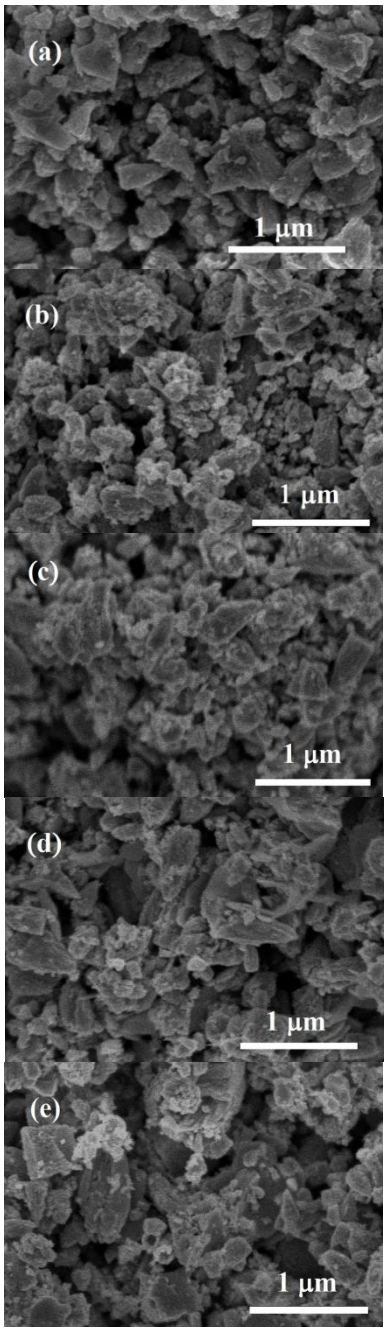

Figure 2. SEM images of (a) as-deposited ZnO films and annealed at different temperatures of (b) 250 °C, (c) 275 °C, (d) 300 °C, and (e) 325 °C

where hv is photon energy, B is a constant, E_g is the optical band gap, and α is the absorption coefficient. The Eg values were determined by the extrapolation of the straight line of $(\alpha hv)^2$ versus hv curve intersecting the horizontal axis. The band gap values of the ZnO films annealed at various temperatures are shown in Table 3.

Based on the results given in Table 3, the band gap values vary with the annealing temperature. It can be seen

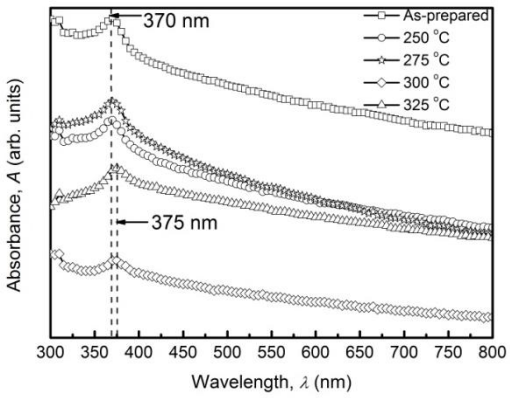

Figure 3. UV-Visible absorbance spectra of the ZnO films annealed at different temperatures

TABLE 3. The optical parameters of the ZnO films annealed at various temperatures

Sample	E_g (eV)	E_{tail} (eV)
As-prepared	3.40	0.211
250 °C	3.25	0.183
275 °C	3.23	0.138
300 °C	3.20	0.262
325 °C	3.18	0.281

that the band gap energy of the as-prepared film (3.40 eV) shifts as compared to the reported value of bulk ZnO (3.37 eV). This can be related to the quantum confinement effect of the nanoparticles. The estimated band gap values show a slight decrease from 3.40 eV to 3.18 eV after annealing at 325 °C. The band gap can be affected by the change in charge carrier concentration and described by Burstein-Moss shift or band gap narrowing effect [25]. The widening of the optical band gap is due to the blocking of lower states of the conduction band for higher charge carrier content in the band filling. The narrowing of band gap is related with various interactions between the charge carriers in the conduction band and valence band. This condition is known as band gap renormalization [26]. These effects can exist simultaneously results in the reduction of the optical band gap. In addition, the annealing temperature may induce the decrease in the optical band gap of ZnO films. This is due to the removal of defects and affecting induced strain in the films. The annealing process also can eliminate the stacking faults resulting in higher crystallite orientation and the reduced-defect in the crystal structure [27].

In amorphous and polycrystalline semiconductors, a band tail can occur in the forbidden energy band gap. This tail appears due to the presence of defects in the semiconductors. The width of band tails of the

electron states can be estimated using the Urbach equation as shown in Equation (11) [28−29].

$$\alpha = \alpha_o \exp\left(\frac{h\nu - E_i}{E_{tail}}\right) \quad (11)$$

where α_o and E_i are constants, E_{tail} is the Urbach energy corresponding to the width of the band tails of electron states. Figure 4 shows photon energy dependence on the absorption coefficient. The Etail can be determined from the reciprocal gradient of the linier portion of these curves in the lower photon energy region. The estimated values of E_{tail} are given in Table 3.

3. 4. Photoluminescence Studies To clarify the different defects and study their evolution with the annealing temperatures, a Gaussian curve fitting was performed for each spectrum, and the estimated values of the peak parameters were obtained. Figures 5(a)-5(f) represent both the defect-related luminescence and Gaussian deconvolutions of the PL spectra for the as-prepared and annealed ZnO films at different temperatures.

There are five UV emission bands (peak 1) correspond to the NBE transition observed at 380 nm, 381 nm, 384 nm, 383 nm, and 380 nm for as-prepared and annealed ZnO films at 250, 275, 300, and 325 °C, respectively. This result shows that the PL intensity of the UV peaks gradually decreases with the increase of annealing temperatures. The decrease in the PL intensities from the samples is probably related to better crystallinity and the reduction of defects in the ZnO films after annealing, which is in accord with the XRD results. The UV peaks of ZnO films in the PL spectra at room temperature are usually located at 380 nm (~3.26 eV) based to literature [30]. Peak 2 shows low-intensity violet emission located on the wavelength of 416 nm for the as-prepared ZnO film. This emission comes from the transition of electrons from the lowest conduction band to the energy level of the zinc vacancies (V_{Zn}). The blue

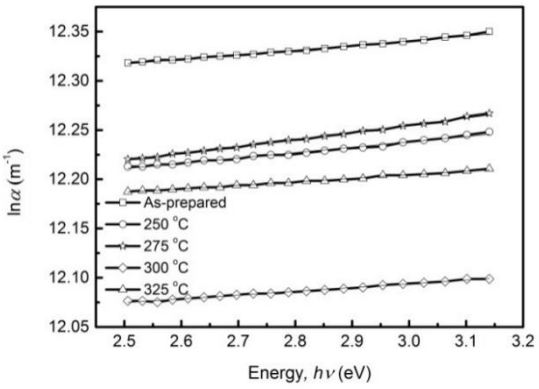

Figure 4. Urbach's plots of the ZnO films annealed at different temperatures

emission (peak 3) has been observed between the wavelengths of 441 nm and 442 nm which is probably attributed to the recombination of excitons between the electrons localized at the zinc interstitial (Zn_i) and the holes in the valence band [31−32]. An increase in annealing temperature up to 325 °C, the blue emission shifts to the higher wavelength (red-shift) centered at the wavelength of 445 nm. It can be seen from Figure 5(b), the emission peak at 466 nm (2.7 eV) can be related to the electronic transition from the donor level of Zni to the acceptor level of V_{Zn} (about 2.6 eV) [33].

The green emission is generally observed in ZnO with the wavelength in the range of 495-570 nm. This can be associated to the recombination of holes and electrons occupying the oxygen vacancies (V_o) related to the defects [34]. Oxygen vacancies (V_o) in ZnO play important key for the occurrence of the green emission. Oxygen vacancies can occur in three different charge states in ZnO. Those are the neutral oxygen vacancy (V_o^0), the singly ionized oxygen vacancy (V_o^+), and the doubly ionized oxygen vacancy (V_o^{++}) originated from the captured two electrons, the captured one electron, and non-captured any electrons with respect to the lattice, respectively [34−35]. Moreover, it has been reported the mechanism responsible for the green emission is due to the recombination of V_o^+ electrons with holes in the valence band. In the present result, the green emission with a slightly longer wavelength is observed when the defects have lower energies in the band gap than those of the V_o^+ state. In this case, the presence of V_o^+ and V_o^{++} states corresponds to the broad green emission having peaks around 544 nm and 570 nm, respectively. In general, the green emission can be attributed to the transition related to V_o [34−35].

The higher PL intensity of the green emission results in the more singly ionized oxygen vacancies of the defects. Some authors have reported that oxygen antisite defects (O_{Zn}) are responsible for the green emission [33−34]. However, the present results show that oxygen vacancies have dominant effect on the green emission. This is probably because the heat treatment in air at different annealing temperatures increases the oxygen in-take into the ZnO films removing both oxygen and zinc vacancies. Consequently, the green emission decreases more rapidly than the blue one. It is also shown that at a low annealing temperature, the PL intensity of the green emission decreases in the ZnO films.

Further, the yellow emission bands (570-590 nm) is affected by the trapped oxygen vacancies. In this case, the holes in the valence band can be trapped at the oxygen vacancy sites and the electron can be trapped at the Zni from the conduction band. Then, the recombination of the holes and the electrons can exhibit yellow emission [35]. The orange emission bands from 590 nm to 620 nm were observed and it is expected to be related to the atomic defects due to interstitial oxygen (O_i) [36].

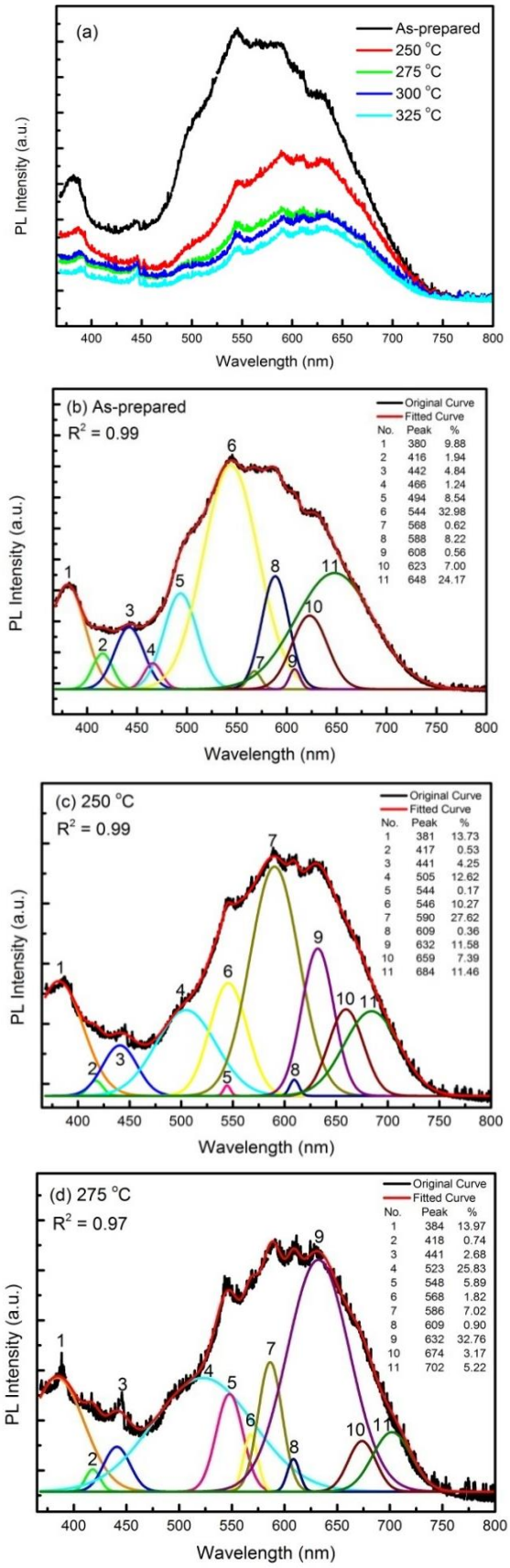

Figure 5. Room temperature PL spectra of (a) as-prepared ZnO films and annealed at different temperatures. In (b), (c), (d), (e), and (f) curves (red color) show the Gaussian deconvolution of experimentally obtained curves and peak positions marked as 1 to 12 show the individual Gaussian curves. The relative content of defects can be obtained from the Gaussian peak separation displayed in the inserted table in the Figures

Meanwhile, the red emission (620-750 nm) may possibly be associated to interstitial oxygen (O_i). From the viewpoint of solid state physics, it is known that Zni and V_o contribute to the formation of free electrons (i.e. donor) in ZnO crystals, whereas V_{Zn}, O_i, and O_{Zn} may consume the free electrons (i.e. acceptor) due recombination process [37, 38]. The relative content of donors and acceptor can be obtained by the peak separation as shown in Figures 5(b)-5(f). It determines the electronic states of ZnO films.

Figure 6 shows the annealing temperature dependence of the relative defect content in the ZnO films. An increase in annealing temperatures from 225 °C to 300 °C enhances the ultraviolet (NBE) emission peak. Meanwhile, the increase of temperatures up to 250 °C, the yellow emission becomes dominant, and the intensity of the blue-green and the orange-red emission decreases. Moreover, it appears that the orange-red emission dominates in the visible spectra indicating that the interstitial oxygen are the dominant defects for these films.

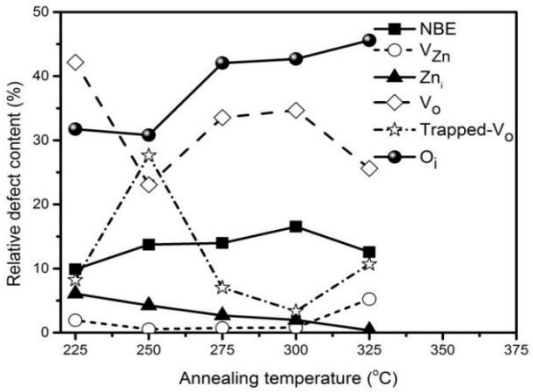

Figure 6. Plot of the relative defect content of the ZnO films prepared for various annealing temperatures

4. CONCLUSIONS

ZnO nanostructured films were successfully prepared onto glass substrate using spin coating method and the effect of annealing on structural and optical properties was studied. The XRD analyses show the polycrystalline structure for as-prepared and annealed ZnO films with preferred crystal orientation along (101) plane. Further, an increase in the structural properties such as lattice parameters and unit cell volume are observed with increasing annealing temperatures. The crystallinity of ZnO films is improved after annealing at 300 °C. The grain size of the as-prepared and annealed ZnO films observed by SEM images are found to be in the range of 31-36 nm. The optical studies show that the red-shift in the band gap energy was observed from the shift in the absorption band edge towards the longer wavelength region. The PL spectra of the films show near band edge (NBE) emission and defects correspond to the visible emissions including V_{Zn}, Zn_i, V_o, trapped-V_o, and O_i, in which the Oi and Vo have dominant effect on ZnO films.

5. ACKNOWLEDGEMENTS

The Authors gratefully acknowledge the use of research facilities of Graduate School of Science and Technology, Laboratory of Semiconductor Device, Kumamoto University, Japan. One of the authors (SYP) also expresses sincere thanks for the financial support funded by DIKTI Scholarship Program from Indonesian government for the graduate program.

6. REFERENCES

1. Tzeng Lue, J., "Physical properties of nanomaterials", ***Encyclopedia of Nanoscience and Nanotechnology***, Vol. X. H.S. Nalwa (Ed.), (2007), 1-46.
2. Özgür, Ü, Alivov, Y. I., Liu, C., Teke, A., Reshchikov, M. A., Dogan, S., Avrutin, V., Cho, S. J., Morkoç, H. "A comprehensive review of ZnO materials and devices", ***Journal of Applied Physics***, Vol. 98, (2005), 041301-041301.
3. Al-Kahlout, A., "ZnO nanoparticles and porous coatings for dye-sensitized solar cell application: Photoelectrochemical characterization", ***Thin Solid Films***, Vol. 520, No. 6, (2012), 1814-1820.
4. Vaezi, M. R. and Zameni, M., "Synthesis of zinc oxide nanostructured thin film by sol-gel method and evaluation of gas sensing properties", ***International Journal of Engineering Transactions B: Applications***, Vol. 27, No. 5, (2014), 757-762.
5. Bhatia, S., Verma, N. and Bedi, R. K., "Ethanol gas sensor based upon ZnO nanoparticles prepared by different techniques", ***Results in Physics***, Vol. 7, (2017), 801-806.
6. Qin, W., Li, T., Li, Y., Qiu, J., Xianjunma, Chen, X., Hu, X. and Zhang, W., "A high power ZnO thin film piezoelectric generator", ***Applied Surface Science***, Vol. 364, (2016), 670-675.
7. Sandeep, K. M., Bhat, S. and Dharmaprakash, S. M., "Structural, optical, and LED characteristics of ZnO and Al doped ZnO thin films", ***Journal of Physics and Chemistry of Solids***, Vol. 104, (2017), 36-44.
8. Lin, B., Fu, Z. and Jia, Y., "Green luminescent center in undoped zinc oxide films deposited on silicon substrates", ***Applied Physics Letters***, Vol. 79, No. 7, (2001), 943-945.
9. Mao, Y. Z., Ma, S.Y., Li, W. Q., Xu, X. L., Gengzang, D.J., Luo, J. and Cheng, L., "Synthesis of porous spherical ZnO nanoparticles and measurement of their gas-sensing property", ***Materials Letters***, Vol. 134, (2014), 80-83.
10. Ying, M., Wang, S., Duan, T., Liao, B., Zhang Y. and Mei, Z., "The structure, optical and magnetic properties of arsenic implanted ZnO films prepared by molecular beam epitaxy", ***Materials Letters***, Vol. 171, (2016), 121-124.
11. Meng, X., Lin, B. and Fu, Z., "Influence of CH3COO– on the room temperature photoluminescence of ZnO films prepared by CVD", ***Journal of Luminescence***, Vol. 126, No. 1, (2007), 203-206.
12. Pflitsch, C., Nebatti, A., Brors, G. and Atakan, B., "MOCVD-growth of thin zinc oxide films from zinc acetylacetonate and air," ***Journal of Crystal Growth***, Vol. 348, No. 1, (2012), 5-9.
13. Purohit, A., Chander, S., Sharma, A., Nehra, S. P. and Dhaka, M. S., "Impact of low temperature annealing on structural, optical, electrical and morphological properties of ZnO thin films grown by RF sputtering for photovoltaic applications", ***Optical Materials***, Vol. 49, (2015), 51-58.
14. Heidari, A., Zinatizadeh, A. A. L. and Younesi, H., "Controllable synthesis of flower-like ZnO nanostructure with hydrothermal method", ***International Journal of Engineering Transactions B: Applications***, Vol. 22, No. 3, (2009), 283-290.
15. Dahnoun, M., Attaf, A., Saidi, H., Yahia, A. and Khelifi, C., "Structural, optical and electrical properties of zinc oxide thin films deposited by sol-gel spin coating technique," ***Optik - International Journal for Light and Electron Optics***, Vol. 134, (2017), 53-59.
16. Heredia, E., Bojorge, C., Casanova, J., Cánepa, H., Craievich, A. and G. Kellermann, "Nanostructured ZnO thin films prepared by sol–gel spin-coating", ***Applied Surface Science***, Vol. 317, (2014), 19-25.
17. Kumar V., Kumar, V., Som, S., Yousif, A., Sigh, A., Ntwaeaborwa, O. M., Kapour A. and Swart, H. C., "Effect of annealing on the structural, morphological and photoluminescence properties of ZnO thin films prepared by spin coating", ***Journal of Colloid and Interface Science***, Vol. 428, (2014), 8-15.

18. Wang, L., Pu, Y., Fang, W., Dai, J., Zheng, C., Mo, C., Xiong, C., Jiang, F., "Effect of high-temperature annealing on the structural and optical properties of ZnO films", ***Thin Solid Films***, Vol. 491, No. 1-2, (2005), 323-327.
19. Cullity, B. D. and Stock, S. R. "Elements of X Ray Diffraction", 3rd ed., Prentice Hall, Upper Saddle River, NJ, 2001.
20. Powder Diffraction File 36-1451 for hexagonal Zinc Oxide, Joint Committe on Powder Diffraction Standards-International center for Diffraction Data.
21. Tsoutsouva, M. G., Panagopoulos, C. N., Papadimitriou, D., Fasaki, I. and Kompitsas, M., "ZnO thin films prepared by pulsed laser deposition", ***Materials Science and Engineering: B***, Vol. 176, No. 6, (2011), 480-483.
22. Khorsand Zak, A., Abd. Majid, W. H., Abrishami M. E. and Yousefi, R., "X-ray analysis of ZnO nanoparticles by Williamson–Hall and size–strain plot methods", ***Solid State Sciences***, Vol. 13, No. 1, (2011), 251-256.
23. Sahai, A. and Goswami, N., "Structural and vibrational properties of ZnO nanoparticles synthesized by the chemical precipitation method", ***Physica E***, Vol. 58, (2014), 130-137.
24. Narayanan, G. N, Sankar Ganesh, R. and Karthigeyan, A., "Effect of annealing temperature on structural, optical and electrical properties of hydrothermal assisted zinc oxide nanorods", ***Thin Solid Films***, Vol. 598, (2016), 39-45.
25. Singh, R.G., Singh, F., Kumar, V. and Mehra, R. M., "Growth kinetics of ZnO nanocrystallites: Structural, optical and photoluminescence properties tuned by thermal annealing", ***Current Applied Physics***, Vol. 11, (2011), 624-630.
26. Abdolahzadeh Ziabari, A. and Rozati, S. M., "Carrier transport and bandgap shift in n-type degenerate ZnO thin films: The effect of band edge nonparabolicity", ***Physica B: Condensed Matter***, Vol. 407, No. 23, (2012), 4512-4517.
27. Mahmood, A., Ahmed, N., Raza, Q., Khan, T. M., Mehmood, M., Hassan, M and Mahmood N., "Effect of thermal annealing on the structural and optical properties of ZnO thin films deposited by the reactive e-beam evaporation technique", ***Physica Scripta***, Vol. 82, No. 6, (2010), 065801.
28. Kazmerski, L., "Polycrystalline and Amorphous Thin Films and Devices", Elsevier, (2012).
29. Motallebi Aghgonbad, M. and Sedghi, H., "Influence of annealing temperature on optical properties of zinc oxide thin films analyzed by spectroscopic ellipsometry method", ***Chinese Journal of Physics***, Vol. 56, (2018), 2129-2138.
30. Li, Y., Cheng, G. S. and Zhang, L. D., "Fabrication of highly ordered ZnO nanowire arrays in anodic alumina membranes". ***Journal of Materials Research***, Vol. 15, No. 11, (2000), 2305-2308.
31. Chaitra, U., Dhananjaya Kekuda and Mohan Rao, K., "Effect of annealing temperature on the evolution of structural, microstructural, and optical properties of spin coated ZnO thin films", ***Ceramic International***, Vol. 43, (2017), 7115-7122.
32. Onofre, Y.J., de Castro, S. and de Godoy, M. P. F., "Effect of traps localization in ZnO thin films by photoluminescence spectroscopy", ***Materials Letters***, Vol. 188, (2017), 37-40.
33. Niu, W., Zhu, H., Wang, X., Ye, J., Song, F., Zhou, J., Gu, S., Shi, Y., Xu, Y. and Zhang, R., "Identification of defect-related emissions in ZnO hybrid materials", ***Applied Physics Letters***, Vol. 107, No. 2, (2015), 021902.
34. Hu, H., Huang, X., Deng, C., Chen, X. and Qian, Y., "Hydrothermal synthesis of ZnO nanowires and nanobelts on a large scale", ***Materials Chemistry and Physics***, Vol. 106, No. 1, (2007), 58-62.
35. Mishra, S. K., Srivastava, R. K., Prakash, S. G., Yadav, R. S. and Panday, A. C., "Photoluminescence and photoconductive characteristics of hydrothermally synthesized ZnO nanoparticles", ***Opto-Electronics Review***, Vol. 18, No. 4, (2010), 467-473.
36. Tsai, C. H., Wang, W. C., Jenq, F. L., Liu, C. C., Hung C. I. and Houng M. P., "Surface modification of ZnO film by hydrogen peroxide solution", ***Journal of Applied Physics***, Vol. 104, No. 5, (2008), 053521.
37. Kwok, W. M., Djuríšić, A. B., Leung, Y. H., Li, D, Tam, K. H., Phillips, D. L., Chan, W. K., "Influence of annealing on stimulated emission in ZnO nanorods", ***Applied Physics Letters***, Vol. 89, No. 18, (2006), 183112.
38. Wu, X. L., Siu, G. G., Fu, C. L. and Ong, H. C., "Photoluminescence and cathodoluminescence studies of stoichiometric and oxygen-deficient ZnO films", ***Applied Physics Letters***, Vol. 78, No. 16, (2001), 2285-2287.

Persian Abstract

چکیده

سنتز فیلم های نانوساختارهای ZnO بروش رسوب دهی پردازش شده بر روی یک بستر شیشه ای با روش پوشش اسپین انجام گردید. تأثیر دمای آنیل شدن (از ۲۵۰ تا ۳۲۵ درجه سانتیگراد به مدت ۳۰ دقیقه) بر روی خصوصیات ساختاری و نوری فیلمهای ZnO بررسی شده است. مطالعات ساختاری نشان می دهد که فیلم های ZnO با ساختار وورتزیت شش ضلعی چند کریستالی هستند. داده های پراش پرتو X (XRD) تبلور بهتری در (۱۰۱) صفحه کریستالی برای فیلم های آنیل در ۳۰۰ درجه سانتیگراد نسبت به سایر فیلم های ZnO نشان می دهد. با افزایش درجه حرارت آنیل ، میانگین اندازه دانه (از ۳۱ به ۳۶ نانومتر) افزایش می یابد. انرژی شکاف باند تقریباً ۳.٤eV برای فیلم های آماده شده است و با افزایش درجه آنیل از ۳.۲۵ به ۳.۱۸ eV متغیر است. نتایج حاصل از تابش نور (PL) میزان انتشار اشعه ماوراء بنفش ضعیف و نسبتاً گسترده را با توجه به ساختارهای مختلف نقص در فیلمهای ZnO نشان می دهد ، که در آن اکسیژن بینابینی و خالی عوامل اصلی مؤثر بر خواص الکترونیکی در کل فیلمهای ZnO هستند.